

Long-range Cooper pair splitting Enhanced by Supercurrent

Wei Chen,^{1,*} D. N. Shi,¹ and D. Y. Xing²

¹College of Science, Nanjing University of Aeronautics and Astronautics, Nanjing 210016, China

²National Laboratory of Solid State Microstructures and Department of Physics, Nanjing University, Nanjing 210093, China

We investigate crossed Andreev reflection (CAR) in a long-range normal metal-superconductor-normal metal junction, with the superconductor carrying a supercurrent along the junction. The energy splitting of quasiparticles in the superconductor induced by the supercurrent opens an energy window, in which CAR can occur over a distance between two normal leads much larger than the superconducting coherence length, with another nonlocal process of elastic cotunneling being completely quenched. As a result, CAR is significantly enhanced within the energy window, and dominates the nonlocal transport, which can be directly measured by the nonlocal differential conductance. The nonlocal entangled electron pairs generated via inverse CAR may belong to opposite or equal energy levels beyond the tunneling limit, and the total entanglement production rate within a unit bias voltage is solely determined by the CAR probability as $\mathcal{P} = 2(1 - A_2)A_2/h$. Our work indicates that a long-range Cooper pair splitter with high efficiency of nonlocal entanglement production can be implemented by simply driving a supercurrent.

PACS numbers: 74.45.+c, 73.20.-r, 03.65.Ud

Introduction.—Quantum entanglement, a kind of nonlocal correlation [1], has important applications in modern quantum information and computation science [2]. Unlike the experimental progresses achieved by photons [3], generation and detection of electron entanglement in solid state physics remains challenging. Among several theoretical proposals, Cooper pairs in the conventional BCS superconductor are considered as a natural source of spin entanglement. Through crossed Andreev reflection (CAR) [4, 5], Cooper pairs can be extracted coherently into different normal terminals, while keeping their spins entangled [6, 7]. Recent experiments on CAR have already shown the feasibility of a Cooper pair splitter [8–16]. In order to probe entanglement, such as Bell-inequality tests [17–23] and other schemes [24, 25], high purity of the nonlocal current contributed by CAR is required. Unfortunately, in the usual normal metal-superconductor hybrid systems, another nonlocal process of elastic cotunneling (EC) occurs ubiquitously, which cancels the nonlocal CAR current in the tunneling limit [26], and can even dominate the nonlocal transport in more transparent junctions [27].

In order to enhance CAR and inhibit EC, several proposals have been put forward, using the spin [5] and energy [28, 29] filtering effects, low-energy collective excitations [30], ac bias [31], Coulomb interaction [6], high-temperature superconductors [32], multiple scattering [33] and also the helical edge states in the topological insulators [29, 34, 35]. Although most proposals predict a CAR dominant nonlocal current, the CAR efficiency is still very low. Moreover, some of them can not be exploited as a spin entangler, since the spin entanglement gets destructed during CAR [5, 34]. Another constraint on a Cooper pair splitter is the distance L between two normal metal-superconductor interfaces must be comparable with the superconducting coherence length $\xi_0 = \hbar v_F/\Delta$. When $L > \xi_0$, CAR probability always decays as $\exp(-L/\xi_0)$ [26]. Therefore, looking for a long-range Cooper pair splitter with high CAR efficiency is of great importance for both detection and application of electronic entanglement.

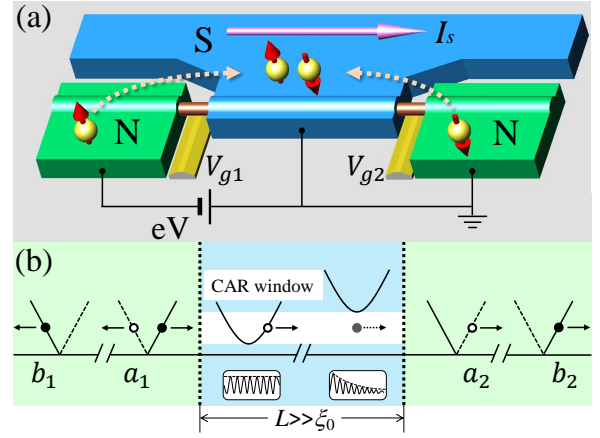


FIG. 1. (color online) (a) Illustration of the normal metal-superconductor-normal metal (NSN) junction fabricated on a nanowire. A supercurrent I_s sketched by the long pink arrow is driven in the S. Two electrons (yellow balls with their spins labeled by the red arrows) from different N regions enter into S and form a Cooper pair during the CAR process. The interface barriers can be tuned by two gates (the golden bars). (b) The quasiparticle picture of CAR, with the filled (open) circles representing the electron-like (hole-like) quasiparticles. The supercurrent modifies the gaps in S and opens a CAR window as shown by the blank region. The free wave of hole-like quasiparticle and evanescent wave of electron-like quasiparticle are sketched by the inserted boxes.

In this Letter, we demonstrate that long-range Cooper pair splitting can be implemented in a normal metal-superconductor-normal metal (NSN) junction by simply driving a supercurrent in the superconductor, as sketched in Fig. 1(a). In the supercurrent-carrying state, Cooper pairs possess a finite momentum, inducing an opposite shift of the gaps for the electron-like and hole-like quasiparticles as shown in Fig. 1(b). As a result, when an electron is incident within the energy window (referred as CAR window) between the two modified gaps, the hole-like quasiparticle is able to propagate

freely in the superconductor, supporting a long-range CAR, while the electron-like quasiparticle decays as the usual case, indicating a suppression of EC. It is shown that the probability of CAR oscillates with the length L of the S region in the CAR window and is significantly enhanced, which can be directly measured through the nonlocal current due to the absence of EC in the long junction limit. Moreover, the generated entangled states via the inverse CAR process are investigated beyond the tunneling regime. Interestingly, we find that there exist two types of spin singlet states, with the entangled electron pairs possessing opposite or equal energies relative to the chemical potential of the superconductor. The total entanglement production rate depends solely on the probability of CAR and is able to achieve large values.

Long-range CAR.-To be specific, we first analyze the CAR in a nanowire NSN junction as shown in Fig. 1(a), where an effective pair potential is induced in the S region due to the proximity effect of the s-wave superconductor. When the superconductor carries a supercurrent I_s , the effective order parameter in the nanowire takes the form of Δe^{2iqx} [36], where the Cooper pair momentum $2q$ can be tuned by the supercurrent through $q = i_s/\xi_0$, with the reduced supercurrent $i_s = I_s/I_c$ normalized by its critical value I_c . We here assume the radius of the nanowire is small compared with the superconducting coherence length ξ_0 , so that the penetration of the pair potential into the N region can be neglected. The whole system can be well described by the following Bogoliubov-de Gennes Hamiltonian [37] as

$$\mathcal{H} = \begin{pmatrix} -\frac{\hbar^2}{2m}\partial_x^2 - \mu + U(x) & i\sigma_y\Delta(x) \\ -i\sigma_y\Delta^*(x) & \frac{\hbar^2}{2m}\partial_x^2 + \mu - U(x) \end{pmatrix}, \quad (1)$$

where σ_y is the spin Pauli matrix, μ is the chemical potential and the pair potential is expressed by the Heaviside step function as $\Delta(x) = \Delta e^{2iqx}\Theta(x)\Theta(L-x)$. The Dirac-type interface barriers of $U(x) = U_1\delta(x) + U_2\delta(x-L)$ are introduced to model the barriers at the NS interfaces [38], which can be tuned by the gates $V_{g1,2}$ as shown in Fig. 1(a). We here assume that a single transverse mode is relevant in the typical energy scale, while the theory can be generalized directly to multiple modes situation.

The Hamiltonian Eq. (1) in the S region can be diagonalized under the plane wave ansatz $(ue^{i(k+q)x}, ve^{i(k-q)x})^T$. The corresponding excitation energy around $\pm k_F$ can be obtained as $E = \pm i_s\Delta + \sqrt{(\hbar v_F\delta k_{\pm})^2 + \Delta^2}$ under the conditions of $q \ll k_F$ and $\Delta \ll \mu$, where the small wave vectors are denoted by $\delta k_{\pm} = k \mp k_F$. The energy spectra manifest that the excitation gaps around the Fermi points $\pm k_F$ shift by an opposite value of $\pm i_s\Delta$ proportional to the supercurrent, as illustrated in Fig. 1(b). Such energy splitting opens a CAR window $E/\Delta \in (1 - i_s, 1 + i_s)$, which provides an opportunity to enhance the CAR by filtering out the EC. To see this point clearly, we solve the scattering problem corresponding to a spin-up electron incident from the left side of the NSN junction with an energy E . The wave functions for all NSN

regions are given by

$$\begin{aligned} \Psi_N^L &= \begin{pmatrix} 1 \\ 0 \end{pmatrix} e^{ik_F x} + a_1 \begin{pmatrix} 0 \\ 1 \end{pmatrix} e^{ik_F x} + b_1 \begin{pmatrix} 1 \\ 0 \end{pmatrix} e^{-ik_F x}, \\ \Psi_N^R &= b_2 \begin{pmatrix} 1 \\ 0 \end{pmatrix} e^{ik_F x} + a_2 \begin{pmatrix} 0 \\ 1 \end{pmatrix} e^{-ik_F x}, \\ \Psi_S &= \sum_{\tau=\pm} \lambda_{\tau} \begin{pmatrix} u_{\tau} \\ v_{\tau} \end{pmatrix} e^{\tau ik_F(1+\beta_{\tau})x} + \chi_{\tau} \begin{pmatrix} v_{\tau} \\ u_{\tau} \end{pmatrix} e^{\tau ik_F(1-\beta_{\tau})x}, \end{aligned} \quad (2)$$

where the electron and hole wave components around $\pm k_F$ are given by $u_{\pm} = \frac{1}{\sqrt{2}}[1 + \sqrt{(E \mp i_s\Delta)^2 - \Delta^2}/(E \mp i_s\Delta)]^{\frac{1}{2}}$ and $v_{\pm} = \sqrt{1 - u_{\pm}^2}$, respectively, and the exponential factor is defined by $\beta_{\pm} = \sqrt{(E \mp i_s\Delta)^2 - \Delta^2}/(2\mu)$. The scattering amplitudes a_1, a_2, b_1, b_2 denote the AR, CAR, normal reflection and EC, respectively, as shown in Fig. 1(b).

All the scattering amplitudes are solved through the boundary conditions of $\Psi_N = \Psi_S$ and $\partial_x \Psi_S - \partial_x \Psi_N = \pm 2k_F Z_j \Psi_S$ at two NS interfaces, with the “ \pm ” and the index $j(=1, 2)$ corresponding to the interfaces at $x = 0, L$, respectively. The dimensionless barrier strength is defined by $Z_j = mU_j/(\hbar^2 k_F)$. When the right NS interface is transparent, the CAR amplitude takes a simple form of

$$a_2 = \frac{i \sin \varphi_2 f(\varphi_1) Z_1}{f(\varphi_1) f(\varphi_2) Z_1^2 - g(\varphi_1) g(\varphi_2) (1 + Z_1^2)}, \quad (3)$$

where the auxiliary functions are defined by $f(x) = \sin(il \sin x)$, $g(x) = \sin(il \sin x - x)$ with the length of the S region being normalized as $l = L/\xi_0$, and the energy dependent phases are defined by $\varphi_{1,2} = \cos^{-1}(E/\Delta \mp i_s)$ when $E/\Delta \mp i_s \leq 1$, and $\varphi_{1,2} = -i \cosh^{-1}(E/\Delta \mp i_s)$ when $E/\Delta \mp i_s > 1$.

When the incident energy is within the CAR window, the exponential factors β_+ and β_- in Eq. (2) take image and real values, respectively, which correspond to an evanescent wave of the electron-like quasiparticle in the $+k_F$ branch and a free wave of the hole-like quasiparticle in the $-k_F$ branch. For a transparent right NS interface, the propagations of the electron-like and hole-like quasiparticles directly contribute to the CE and CAR processes, for no branch-crossing process occurs at the right interface. As a result, only the CAR process survives in the long-range limit $L \gg \xi_0$, with its efficiency well improved simultaneously. The width of the CAR window $2i_s\Delta$ can be adjusted conveniently by the supercurrent. The numerical results of the CAR probability $A_2 = |a_2|^2$ as a function of i_s and E is shown in Fig. 2(a). One can see there exists a notable region confined by the boundaries approximately described by $E/\Delta = 1 \pm i_s$, where CAR gets effectively enhanced. The CAR window can be broadened to a maximal width of 2Δ when a critical supercurrent is driven. At the resonant energy levels, the CAR probability can reach the value of 38%. In Fig. 2(b), we compare the CAR probability A_2 and EC probability $B_2 = |b_2|^2$ before and after the supercurrent being driven. When $i_s = 0$ for a usual

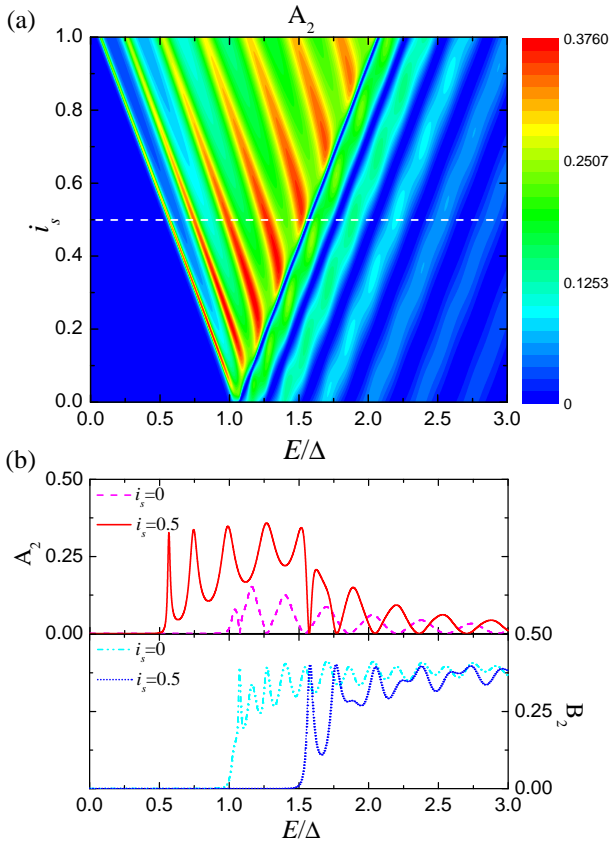


FIG. 2. (color online) (a) The probability of CAR as a function of supercurrent i_s and energy E . (b) The probabilities of CAR and EC before and after the supercurrent being driven. The relevant parameters are set as $L = 8\xi_0$, $Z_1 = 1.25$, $Z_2 = 0$, $k_F = 100/\xi_0$.

NSN junction, both processes are suppressed within the initial gap Δ due to the subgap decay of the normal and anomalous propagators in the S region, while EC dominates the nonlocal transport above the gap. Impressively, when a supercurrent $i_s = 0.5$ is driven, long-range CAR occurs within the CAR window $E/\Delta \in (0.5, 1.5)$ with EC being quenched below the modified gap 1.5Δ . This is a new kind of energy filtering effect, which occurs in the superconductor, in contrast with the previous proposals where the energy filtering is enforced in the normal leads [28]. The advantage of the present scheme is that it will not introduce large mismatch of Fermi velocities in different regions, so that CAR can reach a high efficiency.

It is interesting to investigate the anomalous dependence of the CAR probability on the length of the S region. Within the CAR window, A_2 and B_2 as functions of L are presented in Fig. 3(a). When there is no supercurrent applied, A_2 first increases and then decreases with L , while B_2 monotonically decays with L , as is known for the usual case. After a supercurrent is driven, the result of B_2 changes little, while the situation for A_2 is totally different. A_2 first increases with L to a large value, and then exhibits an oscillation behavior due to the interference between two NS interfaces. In the long-range limit, the CAR amplitude in Eq. (3) reduces to

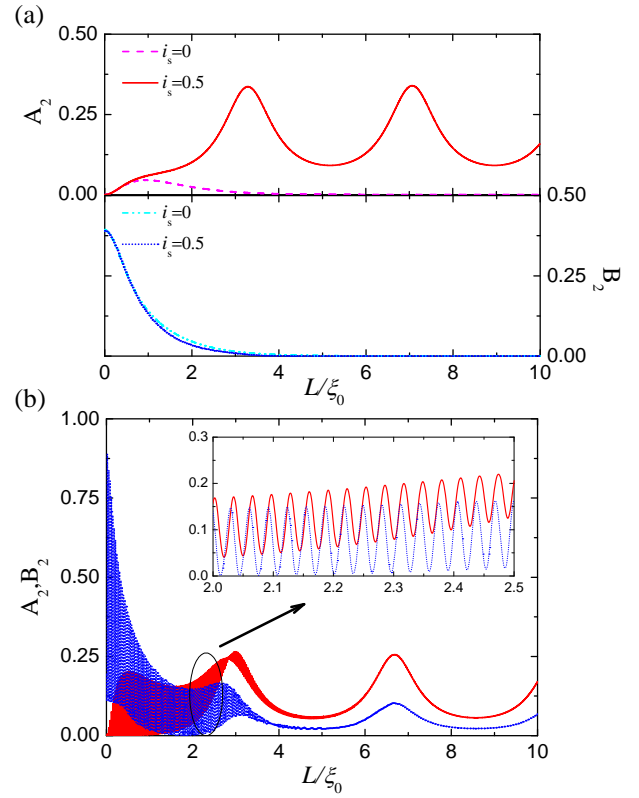


FIG. 3. (color online) The probabilities of CAR and EC as functions of length L for (a) $Z_2 = 0$ and (b) $Z_2 = 0.8$. The relevant parameters are set as $Z_1 = 1.25$, $E/\Delta = 0.8$, $k_F = 100/\xi_0$.

$a_2 = i \sin \varphi_2 Z_1 / [f(\varphi_2) Z_1^2 - e^{i\varphi_1} g(\varphi_2)(1 + Z_1^2)]$ within the CAR window, which corresponds to an oscillating period of $L_0 = \pi\xi_0 / \sinh(i\varphi_2)$. Under the condition of $Z_2 = 0$, the scattering between $\pm k_F$ branches at the right NS interface is absent, thus the period of the oscillation is in scale of ξ_0 . The result for the case of $Z_2 \neq 0$ is shown in Fig. 3(b). In such a case, the scattering with branch-crossing can take place at the right NS interface, so that when $L \sim \xi_0$, A_2 and B_2 exhibit a fast oscillation with the period comparable with $1/k_F$. As L gets larger, the propagation of quasiparticles around $+k_F$ branch can not survive over such a long distance. Therefore, the fast oscillation disappears rapidly and the interference is again contributed purely by the free waves around $-k_F$. Due to the branch-crossing scattering at the right NS interface, the hole-like quasiparticle can now be transferred into an electron in the right lead, resulting in a finite EC probability. It can be proved that the ratio of the EC probability to the CAR probability approximates to $B_2/A_2 = Z_2^2/(1 + Z_2^2)$ for a long junction, so that the nonlocal transport is still dominated by the CAR. In the tunneling limit $Z_2 \gg 1$, the two nonlocal processes cancel each other, coinciding with the conventional results [26].

The CAR can be directly measured by the nonlocal current. By applying a negative bias voltage $eV \in \Delta(1 - i_s, 1 + i_s)$ on the left lead while keeping the superconductor and the

right lead grounded as shown in Fig. 1(a), the nonlocal differential conductance within the CAR window is $G_2/G_0 = A_2/(1 + Z_2^2)$, with $G_0 = e^2/h$ the unit conductance (the positive direction of current is from the leads into the superconductor). The positive nonlocal conductance manifests a CAR dominant nonlocal transport. The dependence of the interface barrier Z_2 on the gate voltage V_{g2} can be calibrated through the normal state transport beforehand, so that the CAR probability can be measured directly by the conductance G_2 .

Entanglement generation via inverse CAR.—The all-electron picture of CAR is that two electrons from different normal lead penetrate into the superconductor by forming a Cooper pair. Inversely, a Cooper pair can break up into two nonlocal spin entangled electrons as well, which can be achieved by imposing a positive bias voltage ($eV < 0$) on the left lead and reversing the direction of the supercurrent at the same time.

Since the CAR occurs with high efficiency, the entangled state should be analyzed beyond the tunneling limit. It turns out that nontrivial results of nonlocal entanglement will appear under such a regime. To see this, we start with the many-body state of incident holes occupying within the energy window from the Fermi level to $|eV|$ in the left N region as $|\Psi_{\text{in}}\rangle = \prod_{0 < E < |eV|} \gamma_{L\uparrow, E}^{\dagger} \gamma_{L\downarrow, E}^{\dagger} |0\rangle$, where $\gamma_{L\sigma, E}^{\dagger}$ generates an incident hole in the left lead with energy E and spin $\sigma (= \uparrow, \downarrow)$, and the vacuum $|0\rangle$ represents the Fermi sea filled up to $E = 0$ in all three regions. The incident and outgoing waves are related by the scattering coefficients [20, 21] through

$$\gamma_{L\sigma}^{\dagger} = b_{1\sigma}^h \gamma_{L\sigma}^{\dagger\text{oh}} + a_{1\sigma}^h c_{L\sigma}^{\dagger\text{oh}} + b_{2\sigma}^h \gamma_{R\sigma}^{\dagger\text{oh}} + a_{2\sigma}^h c_{R\sigma}^{\dagger\text{oh}}, \quad (4)$$

where the operators of the outgoing hole and electron in lead $\alpha (= L, R)$ are $\gamma_{\alpha\sigma}^{\dagger}$ and $c_{\alpha\sigma}^{\dagger}$ with the energy index omitted, and the scattering amplitudes correspond to that in Eq. (2) except the superscript denoting the hole incident case. Substituting Eq. (4) into the expression of $|\Psi_{\text{in}}\rangle$ one arrives at the outgoing state of quasiparticles. In order to obtain the entangled state between electrons, the quasiparticle picture should be transformed into the all-electron picture [20, 39]. This can be done by choosing a new vacuum state $|\tilde{0}\rangle$, which is related to the original one through $|0\rangle = \prod_{eV < E < 0} c_{L\uparrow, E}^{\dagger} c_{L\downarrow, E}^{\dagger} |\tilde{0}\rangle$, and performing a particle-hole transformation as $\gamma_{\alpha\sigma, E}^{\dagger} = c_{\alpha\bar{\sigma}, -E}^{\dagger}$, which says that creating a hole is equivalent to annihilating an electron with opposite energy and spin. Then for the optimal case $Z_2 = 0$, the many-body outgoing state can be obtained as [40]

$$\begin{aligned} |\Psi_{\text{out}}\rangle &= \prod_{0 < E < |eV|} (\kappa |\mathcal{E}\rangle + \tilde{\kappa} |\tilde{\mathcal{E}}\rangle + |\mathcal{O}\rangle) \\ |\mathcal{E}\rangle &= \frac{\sqrt{2}}{2} [c_{R\uparrow, E}^{\dagger} c_{L\downarrow, -E}^{\dagger} - c_{R\downarrow, E}^{\dagger} c_{L\uparrow, -E}^{\dagger}] |\tilde{0}\rangle, \\ |\tilde{\mathcal{E}}\rangle &= \frac{\sqrt{2}}{2} [c_{R\uparrow, E}^{\dagger} c_{L\downarrow, E}^{\dagger} - c_{R\downarrow, E}^{\dagger} c_{L\uparrow, E}^{\dagger}] c_{L\downarrow, -E}^{\dagger} c_{L\uparrow, -E}^{\dagger} |\tilde{0}\rangle, \end{aligned} \quad (5)$$

where $|\mathcal{E}\rangle$ and $|\tilde{\mathcal{E}}\rangle$ are two kinds of nonlocal spin singlet states created during CAR process with the amplitudes of

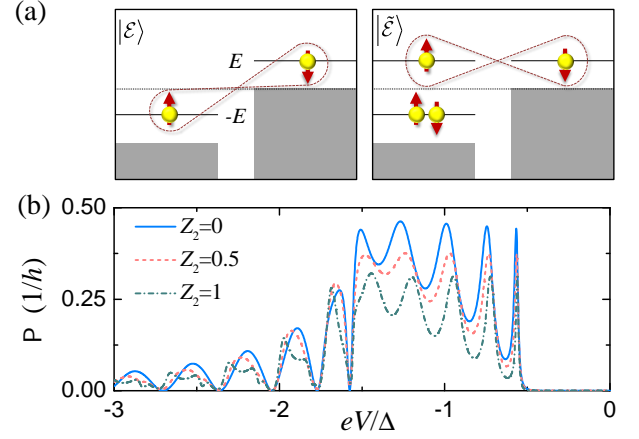


FIG. 4. (color online) (a) Schematic of entangled states between equal and opposite energy levels. (b) Entanglement production rate \mathcal{P} as a function of bias voltage for different Z_2 . The relevant parameters are set as $L = 8\xi_0$, $Z_1 = 1.25$, $i_s = -0.5$, $k_F = 100/\xi_0$.

$\kappa = -\sqrt{2}a_2^*(-E)b_1^*(-E)$ and $\tilde{\kappa} = \sqrt{2}a_1^*(-E)a_2^*(-E)$, respectively, while $|\mathcal{O}\rangle$ includes the other many-body scattered states such as the local entangled state, product states and the vacuum state. During the derivation of Eq. (5) we have taken into account the particle-hole symmetry of the scattering matrix, and expressed the state with the scattering amplitudes for the electron incident case [40].

$|\mathcal{E}\rangle$ is the usual nonlocal entangled state generated by CAR, where two entangled electrons belong to opposite energies [20, 39], as shown in the left panel of Fig. 4(a). This is consistent with the fact that CAR is an elastic process, so that the total energy of the two electrons is conserved during the pair breaking. We note that the amplitude κ reduces to $\sqrt{2}a_2^*$ in the tunneling limit $b_1^* \approx 1$, coinciding with the results in previous literatures [20, 21, 39]. The anomalous entangled state $|\tilde{\mathcal{E}}\rangle$ comes from a higher-order contribution, which appears only when the amplitudes of AR and CAR take considerable values. It seems counterintuitive at first sight that the amplitude of $|\tilde{\mathcal{E}}\rangle$ is proportional to a_1^* , for the competitive process of AR usually reduces the CAR probability. However, this is not the whole story. The coincidence of AR and CAR first results in a double occupation of the energy level $-E$, ruling out the possibility of entanglement therein; then the Fermi statistics of electrons and the opposite spin pairing in the superconductor together result in a nonlocal entangled state with the same energy E , as shown in the right panel of Fig. 4(a). This kind of nonlocal entanglement created during the CAR process has not been discussed before, which appears only under the regime deviating from the tunneling limit.

Given that the rate of the scattering events in a unit energy interval is $1/h$, the total entanglement production rate can be obtained as

$$\mathcal{P}(eV) = 2[1 - \frac{1 + 2Z_2^2}{1 + Z_2^2} A_2] A_2/h, \quad (6)$$

in the CAR window, which is solely determined by the CAR

probability for a long-rang Cooper pair splitter. For the case $Z_2 = 0$, it reduces to $\mathcal{P} = 2(1 - A_2)A_2/h$, which suggests that a saturation value of \mathcal{P} can be reached when $A_2 = 0.5$. Therefore, the efficiency of nonlocal entanglement generation is not a monotone increasing function of the CAR probability beyond the tunneling limit. This is because for a high efficiency of CAR, two entangled pairs generated at one time may destroy the spin entanglement due to the Fermi statistics. The numerical results of \mathcal{P} are shown in Fig. 4(b) for different barrier strength Z_2 . For a transparent right NS interface, \mathcal{P} approaches its saturation value of 0.5 at some resonant levels within the CAR window, which means an ideal entangler can be implemented in our proposal. The existence of the interface barrier Z_2 will suppress the entanglement generation, while a large value of \mathcal{P} can always be expected as long as the barrier Z_2 is not very strong.

The nonlocal spin entanglement of states $|\mathcal{E}\rangle$ and $|\tilde{\mathcal{E}}\rangle$ can be demonstrated through either the violation of the Bell inequality [18–23] or a well-designed spintronic quantum eraser [24]. Both schemes can be achieved by the measurement on the spin resolved current correlation. Since the state $|\mathcal{O}\rangle$ in Eq. (5) carries no nonlocal correlation, a nonlocal spin correlation contributed purely by $|\mathcal{E}\rangle$ and $|\tilde{\mathcal{E}}\rangle$ can be expected when the right NS interface is transparent. Interestingly, the equal energy entangled state $|\tilde{\mathcal{E}}\rangle$ can also be probed by the bunching behavior in a beam splitter setup [25], since the orbital wave function of the singlet state is symmetric.

Discussions.—Finally, we discuss the experimental realization of our proposal. The long-range Cooper pair splitter as shown in Fig. 1(a) possesses the same configuration as that in the experiments reported in Ref. [11, 14–16], so that it can be implemented by the existing technologies. Moreover, since no quantum dots embedded in the nanowire needs to be fabricated, more kinds of nanowires can be adopted to build the NSN junction. The key point here is a supercurrent flowing along the junction, which can be driven by imposing a constant current on the superconductor or by utilizing a magnetic flux in a superconductor loop. The density of states in the superconductor should be much larger than that in the nanowire, so that the self-consistent modification of the order parameter in the superconductor can be neglected. Possible renormalization of the Fermi velocity due to the superconducting proximity effect can be compensated by a back gate. In order to realize a high-efficiency entangler and extract pure signal of entanglement, the interface barriers $Z_{1,2}$ should be carefully tuned by the gates $V_{g1,2}$. The optimal case corresponding to the voltage bias configuration in Fig. 1(a) occurs when $Z_1 \in (1, 2)$ and $Z_2 = 0$, which can be achieved in the experiment [16]. For the case $Z_2 \neq 0$, the signal of entanglement will get weakened since the intervention of EC results in an opposite current contribution; nevertheless, since the CAR dominates the nonlocal transport in the CAR window, the signal of entanglement is always extractable.

* weichenphy@nuaa.edu.cn

- [1] A. Einstein, B. Podolsky, and N. Rosen, *Phys. Rev.* **47**, 777 (1935); E. Schrödinger, *Proc. Cambridge Philos. Soc.* **31**, 555 (1935).
- [2] M. A. Nielsen and I. L. Chuang, *Quantum Computation and Quantum Information* (Cambridge University Press, Cambridge, England, 2000).
- [3] A. Aspect, P. Grangier, and G. Roger, *Phys. Rev. Lett.* **47**, 460 (1981); *ibid.* **49**, 91 (1982); W. Tittel, J. Brendel, H. Zbinden, and N. Gisin, *ibid.* **81**, 3563 (1998); A. Zeilinger, *Rev. Mod. Phys.* **71**, S288 (1999).
- [4] J. M. Byers and M. E. Flatté, *Phys. Rev. Lett.* **74**, 306 (1995).
- [5] G. Deutscher and D. Feinberg, *Appl. Phys. Lett.* **76**, 487 (2000).
- [6] P. Recher, E. V. Sukhorukov, and D. Loss, *Phys. Rev. B* **63**, 165314 (2001).
- [7] G. B. Lesovik, T. Martin, and G. Blatter, *Eur. Phys. J. B* **24**, 287 (2001).
- [8] D. Beckmann, H. B. Weber, and H. v. Löhneysen, *Phys. Rev. Lett.* **93**, 197003 (2004).
- [9] S. Russo, M. Kroug, T. M. Klapwijk, and A. F. Morpurgo, *Phys. Rev. Lett.* **95**, 027002 (2005).
- [10] P. Cadden-Zimansky and V. Chandrasekhar, *Phys. Rev. Lett.* **97**, 237003 (2006).
- [11] L. Hofstetter, S. Csonka, J. Nygård, and C. Schönberger, *Nature (London)* **461**, 960 (2009); L. Hofstetter, S. Csonka, A. Baumgartner, G. Fülöp, S. d’Hollosy, J. Nygård, and C. Schönberger, *Phys. Rev. Lett.* **107**, 136801 (2011).
- [12] P. Cadden-Zimansky, J. Wei and V. Chandrasekhar, *Nat. Phys.* **5**, 393 (2009).
- [13] J. Wei and V. Chandrasekhar, *Nat. Phys.* **6**, 494 (2010).
- [14] L. G. Herrmann, F. Portier, P. Roche, A. Levy Yeyati, T. Kontos, and C. Strunk, *Phys. Rev. Lett.* **104**, 026801 (2010).
- [15] J. Schindele, A. Baumgartner, and C. Schönberger, *Phys. Rev. Lett.* **109**, 157002 (2012).
- [16] A. Das, Y. Ronen, M. Heiblum, D. Mahalu, A. V. Kretinin and H. Shtrikman, *Nat. Commun.* **3**, 1165 (2012).
- [17] J. S. Bell, *Physics (Long Island City, N.Y.)* **1**, 195 (1964); J. S. Bell, *Rev. Mod. Phys.* **38**, 447 (1966); J. F. Clauser *et al.*, *Phys. Rev. Lett.* **23**, 880 (1969).
- [18] S. Kawabata, *J. Phys. Soc. Jpn.* **70**, 1210 (2001).
- [19] N. M. Chtchelkatchev *et al.*, *Phys. Rev. B* **66**, 161320(R) (2002).
- [20] P. Samuelsson, E. V. Sukhorukov, and M. Büttiker, *Phys. Rev. Lett.* **91**, 157002 (2003); *ibid.* **92**, 026805 (2004).
- [21] C. W. J. Beenakker, C. Emary, M. Kindermann, and J. L. van Velsen, *Phys. Rev. Lett.* **91**, 147901 (2003); C. W. J. Beenakker, arXiv:cond-mat/0508488v3.
- [22] W. Chen, R. Shen, L. Sheng, B. G. Wang, and D. Y. Xing, *Phys. Rev. Lett.* **109**, 036802 (2012).
- [23] B. Braunecker, P. Bursset, and A. Levy Yeyati, *Phys. Rev. Lett.* **111**, 136806 (2013).
- [24] W. Chen, R. Shen, Z. D. Wang, L. Sheng, B. G. Wang, and D. Y. Xing, *Phys. Rev. B* **87**, 155308 (2013); W. Chen, Z. D. Wang, R. Shen and D. Y. Xing, *Phys. Lett. A* **378**, 1893 (2014).
- [25] G. Burkard, D. Loss, and E. V. Sukhorukov, *Phys. Rev. B* **61**, R16303 (2000).
- [26] G. Falci, D. Feinberg, and F. W. J. Hekking, *Europhys. Lett.* **54**, 255 (2001).
- [27] M. S. Kalenkov and A. D. Zaikin, *Phys. Rev. B* **75**, 172503 (2007).
- [28] J. Cayssol, *Phys. Rev. Lett.* **100**, 147001 (2008); M. Veldhorst

- and A. Brinkman, Phys. Rev. Lett. **105**, 107002 (2010).
- [29] W. Chen, R. Shen, L. Sheng, B. G. Wang, and D. Y. Xing, Phys. Rev. B **84**, 115420 (2011).
- [30] A. Levy Yeyati et al., Nature Phys. **3**, 455 (2007).
- [31] D. S. Golubev and A. D. Zaikin, Europhys. Lett. **86**, 37 009 (2009).
- [32] W. J. Herrera, A. Levy Yeyati, and A. Martin-Rodero, Phys. Rev. B **79**, 014520 (2009).
- [33] M Flöser, D Feinberg, R Mélin, arXiv:1211.5341.
- [34] J. Nilsson, A. R. Akhmerov, and C. W. J. Beenakker, Phys. Rev. Lett. **101**, 120403 (2008).
- [35] R. W. Reinthaler, P. Recher, and E. M. Hankiewicz, **110**, 226802 (2013).
- [36] W. Chen, M. Gong, R. Shen, and D. Y. Xing, arXiv:1311.4652 (2013).
- [37] P. G. de Gennes, *Superconductivity of Metals and Alloys* (Benjamin, New York, 1966).
- [38] G. E. Blonder, M. Tinkham, and T. M. Klapwijk, Phys. Rev. B **25**, 4515 (1982).
- [39] E. Prada and F. Sols, Eur. Phys. J. B, **40**, 379 (2004).
- [40] See Supplemental Material for details.

SUPPLEMENTARY MATERIAL

Particle-hole symmetry of the scattering matrix

In this subsection, we deduce the relation between the scattering amplitudes for the electron and hole incident cases. The second quantized Bogoliubov-de Gennes Hamiltonian is

$$\hat{H} = \int dx \Phi^\dagger(x) \mathcal{H}(x) \Phi(x), \quad (\text{S.1})$$

where the \mathcal{H} is defined by Eq. (1) in the Nambu representation of $\Phi = (\hat{\psi}_\uparrow, \hat{\psi}_\downarrow, \hat{\psi}_\uparrow^\dagger, \hat{\psi}_\downarrow^\dagger)^T$ with ‘‘T’’ representing a matrix transpose. The four-component operator Φ satisfies $(\Phi^\dagger)^T = \tau_x \Phi$ with τ_x the Pauli matrix operating on the particle-hole components. Apply this restriction on Eq. (S.1), one obtains the particle-hole transformation invariance of the Hamiltonian as

$$\mathcal{H} = -\Xi \mathcal{H} \Xi^{-1}, \quad (\text{S.2})$$

where $\Xi = \tau_x K$ is the particle-hole transformation operator and K represents the complex conjugate. As a result, if ψ is an eigenstate of \mathcal{H} of energy E as

$$\mathcal{H}\psi(E) = E\psi(E), \quad (\text{S.3})$$

then we obtain

$$\mathcal{H}\Xi\psi(E) = -E\Xi\psi(E), \quad (\text{S.4})$$

by using Eq. (S.2). This means $\Xi\psi(E) = \psi(-E)$ is an eigenstate of \mathcal{H} as well with energy $-E$.

Next we prove that the particle-hole symmetry of the Hamiltonian \mathcal{H} results in the particle-hole symmetry of the scattering matrix. For the translation invariant system, the eigenstate is a plane wave as

$$\psi_{\eta\sigma}(k, E) = (u_\uparrow, u_\downarrow, v_\downarrow, v_\uparrow)^T e^{i(kx - Et/\hbar)}, \quad (\text{S.5})$$

where η, σ are the particle-hole and spin indexes, respectively. Performing the particle-hole transformation on the wave function leads to

$$\begin{aligned} \Xi\psi_{\eta\sigma}(k, E) &= (v_\downarrow^*, v_\uparrow^*, u_\uparrow^*, u_\downarrow^*)^T e^{-i(kx - Et/\hbar)} \\ &= \psi_{\bar{\eta}\bar{\sigma}}(-k, -E), \end{aligned} \quad (\text{S.6})$$

which means the particle-hole operation results in a flip of both particle-hole and spin components. Importantly, the moving direction of the quasiparticle is invariant for the momentum and energy change their signs simultaneously. Therefore, an incident (outgoing) wave is still an incident (outgoing) wave after the particle-hole transformation.

In general, the incident and outgoing waves can be expressed as

$$\begin{aligned} |\Psi^i\rangle &= \sum_{\alpha\eta\sigma} \tilde{a}_{\alpha\eta\sigma}(E) \psi_{\alpha\eta\sigma}^i(E) \\ |\Psi^o\rangle &= \sum_{\alpha'\eta'\sigma'} \tilde{b}_{\alpha'\eta'\sigma'}(E) \psi_{\alpha'\eta'\sigma'}^o(E), \end{aligned} \quad (\text{S.7})$$

where $\tilde{a}_{\alpha\eta\sigma}(E), \tilde{b}_{\alpha'\eta'\sigma'}(E)$ are the wave amplitudes of the incident and outgoing waves. We have omitted the momentum index, for its sign corresponds to the incident or outgoing waves. The amplitudes of the incident and outgoing waves are related by the scattering matrix as

$$\tilde{b}_{\alpha'\eta'\sigma'}(E) = S_{\eta'\eta,\sigma'\sigma}^{\alpha'\alpha}(E)\tilde{a}_{\alpha\eta\sigma}(E), \quad (\text{S.8})$$

which can be obtained by solving the Bogoliubov-de Gennes equation. $S_{\eta'\eta,\sigma'\sigma}^{\alpha'\alpha}(E)$ is the scattering amplitude for an incident wave in the α lead with a particle-hole component η and spin σ being scattered into an outgoing wave in the α' lead with a particle-hole component η' and spin σ' .

Performing the particle-hole transformation on the wave functions (S.7) results in

$$\begin{aligned} \Xi|\Psi^i\rangle &= \sum_{\alpha\eta\sigma} \tilde{a}_{\alpha\eta\sigma}^*(E)\psi_{\alpha\bar{\eta}\bar{\sigma}}^i(-E) \\ \Xi|\Psi^o\rangle &= \sum_{\alpha'\eta'\sigma'} \tilde{b}_{\alpha'\eta'\sigma'}^*(E)\psi_{\alpha'\bar{\eta}'\bar{\sigma}'}^o(-E). \end{aligned} \quad (\text{S.9})$$

Since the above wave functions still satisfy the same Bogoliubov-de Gennes equation, the amplitudes of the incident and outgoing waves are also related by the same scattering matrix as

$$\tilde{b}_{\alpha'\eta'\sigma'}^*(E) = S_{\eta'\eta,\bar{\sigma}'\bar{\sigma}}^{\alpha'\alpha}(-E)\tilde{a}_{\alpha\eta\sigma}^*(E). \quad (\text{S.10})$$

Note that the sign of the energy in the matrix elements is reversed, for the wave functions after transformation possess an eigenenergy of $-E$. Comparing Eq. (S.8) and Eq. (S.10), we

arrive at the particle-hole symmetry of the matrix as

$$S_{\eta'\eta,\sigma'\sigma}^{\alpha'\alpha}(E) = S_{\eta'\eta,\bar{\sigma}'\bar{\sigma}}^{\alpha'\alpha*}(-E), \quad (\text{S.11})$$

which means that the amplitude for a spin-up (spin-down) incident electron (hole) with an energy E being scattered into a spin-up (spin-down) outgoing electron (hole) equals the amplitude for a spin-down (spin-up) incident hole (electron) with an energy $-E$ being scattered into a spin-down (spin-up) outgoing hole (electron).

Specifically, by adopting the notation of the scattering amplitudes in the main text, which correspond to the matrix elements through $a_1(E) = S_{he,\uparrow\uparrow}^{LL}(E), a_2(E) = S_{he,\uparrow\uparrow}^{RL}(E), b_1(E) = S_{ee,\uparrow\uparrow}^{LL}(E), b_2(E) = S_{ee,\uparrow\uparrow}^{RL}(E)$ and $a_{1\sigma}^h(E) = S_{eh,\sigma\sigma}^{LL}(E), a_{2\sigma}^h(E) = S_{eh,\sigma\sigma}^{RL}(E), b_{1\sigma}^h(E) = S_{hh,\sigma\sigma}^{LL}(E), b_{2\sigma}^h(E) = S_{hh,\sigma\sigma}^{RL}(E)$, and utilizing the relations $S_{\eta'\eta,\sigma'\sigma}^{\alpha'\alpha}(E) = -S_{\eta'\eta,\bar{\sigma}'\bar{\sigma}}^{\alpha'\alpha}(-E), S_{\eta'\eta,\sigma\sigma}^{\alpha'\alpha}(E) = S_{\eta'\eta,\bar{\sigma}\bar{\sigma}}^{\alpha'\alpha}(E)$, the particle-hole symmetry leads to

$$\begin{aligned} a_{1\uparrow}^h(E) &= -a_{1\downarrow}^h(E) = -a_1^*(-E) \\ a_{2\uparrow}^h(E) &= -a_{2\downarrow}^h(E) = -a_2^*(-E) \\ b_{1\uparrow}^h(E) &= b_{1\downarrow}^h(E) = b_1^*(-E) \\ b_{2\uparrow}^h(E) &= b_{2\downarrow}^h(E) = b_2^*(-E). \end{aligned} \quad (\text{S.12})$$

Derivation of the entangled states

In order to obtain the entangled states generated via the inverse CAR, we start with the many-body incident state of $|\Psi_{\text{in}}\rangle = \prod_{0 < E < |eV|} \gamma_{L\uparrow,E}^\dagger \gamma_{L\downarrow,E}^\dagger |0\rangle$, where the incident holes occupy the energy window from the Fermi level to $|eV|$ in the left N region. The many-body outgoing wave can be obtained by expressing the operators of the incident wave by that of the outgoing wave, i.e., Eq. (4) in the main text, which leads to

$$|\Psi_{\text{out}}\rangle = \prod_{0 < E < |eV|, \sigma} [b_{1\sigma}^h(E)\gamma_{L\sigma,E}^{\dagger} + a_{1\sigma}^h(E)c_{L\sigma,E}^{\dagger} + b_{2\sigma}^h(E)\gamma_{R\sigma,E}^{\dagger} + a_{2\sigma}^h(E)c_{R\sigma,E}^{\dagger}]|0\rangle \quad (\text{S.13})$$

Then we introduce a new vacuum state $|\tilde{0}\rangle$, which is related to the original one through $|0\rangle = \prod_{eV < E < 0} c_{L\uparrow,E}^{\dagger} c_{L\downarrow,E}^{\dagger} |\tilde{0}\rangle$.

Inserting this equality into the above equation results in

$$\begin{aligned} |\Psi_{\text{out}}\rangle &= \prod_{0 < E < |eV|, \sigma} [b_{1\sigma}^h(E)\gamma_{L\sigma,E}^{\dagger} + a_{1\sigma}^h(E)c_{L\sigma,E}^{\dagger} + b_{2\sigma}^h(E)\gamma_{R\sigma,E}^{\dagger} + a_{2\sigma}^h(E)c_{R\sigma,E}^{\dagger}] \prod_{eV < E' < 0, \sigma'} c_{L\sigma',E'}^{\dagger} |\tilde{0}\rangle \\ &= \prod_{0 < E < |eV|, \sigma} [b_{1\sigma}^h(E)\gamma_{L\sigma,E}^{\dagger} + a_{1\sigma}^h(E)c_{L\sigma,E}^{\dagger} + b_{2\sigma}^h(E)\gamma_{R\sigma,E}^{\dagger} + a_{2\sigma}^h(E)c_{R\sigma,E}^{\dagger}] c_{L\bar{\sigma},-E}^{\dagger} |\tilde{0}\rangle. \end{aligned} \quad (\text{S.14})$$

By performing the following particle-hole transformation $\gamma_{\alpha\sigma,E}^{\dagger} = c_{\alpha\bar{\sigma},-E}^0$ on the hole operators, we arrive at

$$|\Psi_{\text{out}}\rangle = \prod_{0 < E < |eV|, \sigma} [b_{1\sigma}^h(E)\mathbb{1} + a_{1\sigma}^h(E)c_{L\sigma,E}^{\dagger}c_{L\bar{\sigma},-E}^{\dagger} + b_{2\sigma}^h(E)c_{R\bar{\sigma},-E}^{\dagger}c_{L\bar{\sigma},-E}^{\dagger} + a_{2\sigma}^h(E)c_{R\sigma,E}^{\dagger}c_{L\bar{\sigma},-E}^{\dagger}]\tilde{0}\rangle. \quad (\text{S.15})$$

For the optimal case $Z_2 = 0$, the EC process is completely suppressed in the CAR window, i.e., $b_{2\sigma}^h = 0$, and the many-body outgoing state reduces to

$$|\Psi_{\text{out}}\rangle = \prod_{0 < E < |eV|} (\kappa|\mathcal{E}\rangle + \tilde{\kappa}|\tilde{\mathcal{E}}\rangle + |\mathcal{O}\rangle)$$

$$|\mathcal{E}\rangle = \frac{\sqrt{2}}{2}[c_{R\uparrow,E}^{\dagger}c_{L\downarrow,-E}^{\dagger} - c_{R\downarrow,E}^{\dagger}c_{L\uparrow,-E}^{\dagger}]\tilde{0}\rangle, |\tilde{\mathcal{E}}\rangle = \frac{\sqrt{2}}{2}[c_{R\uparrow,E}^{\dagger}c_{L\downarrow,E}^{\dagger} - c_{R\downarrow,E}^{\dagger}c_{L\uparrow,E}^{\dagger}]c_{L\downarrow,-E}^{\dagger}c_{L\uparrow,-E}^{\dagger}\tilde{0}\rangle,$$

$$\kappa = -\sqrt{2}a_2^*(-E)b_1^*(-E), \tilde{\kappa} = \sqrt{2}a_1^*(-E)a_2^*(-E)$$

$$|\mathcal{O}\rangle = b_1^{*2}(-E)\tilde{0}\rangle - a_1^{*2}(-E)c_{L\uparrow,E}^{\dagger}c_{L\downarrow,E}^{\dagger}c_{L\uparrow,-E}^{\dagger}c_{L\downarrow,-E}^{\dagger}\tilde{0}\rangle - a_2^{*2}(-E)c_{R\uparrow,E}^{\dagger}c_{R\downarrow,E}^{\dagger}c_{L\uparrow,-E}^{\dagger}c_{L\downarrow,-E}^{\dagger}\tilde{0}\rangle - \sqrt{2}a_1^*(-E)b_1^*(-E)|\mathcal{E}\rangle_{\text{local}},$$

$$|\mathcal{E}\rangle_{\text{local}} = \frac{\sqrt{2}}{2}[c_{L\uparrow,E}^{\dagger}c_{L\downarrow,-E}^{\dagger} - c_{L\downarrow,E}^{\dagger}c_{L\uparrow,-E}^{\dagger}]\tilde{0}\rangle, \quad (\text{S.16})$$

where we have used the Eq. (S.12). The states $|\mathcal{E}\rangle$ and $|\tilde{\mathcal{E}}\rangle$ are two kinds of nonlocal entangled states, while the state $|\mathcal{O}\rangle$ is

the superposition of the local entangled state $|\mathcal{E}\rangle_{\text{local}}$, the direct conduct states and the vacuum state.